Unfolding proteins in an external field: Can we always observe the intermediate states?

Alexander S. Lemak, James R. Lepock, and Jeff Z. Y. Chen*
Department of Physics, University of Waterloo, Waterloo, Ontario, Canada N2L 3G1
(Received 2 April 2002; published 19 March 2003)

A protein molecule under the stress of an external denaturing force acting on a terminal end or on the entire molecule is expected to unfold, possibly through a few intermediate stages depending on the magnitude of the denaturing force. We have investigated two protein minimal models under various types of denaturing force fields using the collision molecular-dynamics simulation, in order to critically examine the relationship between the folding pathways observed in different protein denaturing experiments.

DOI: 10.1103/PhysRevE.67.031910 PACS number(s): 87.15.Aa, 82.37.Rs

I. INTRODUCTION

Understanding the complex kinetics of structural transformation in proteins and DNA is one of the most challenging problems in biological physics. The recent progress in experimental techniques has made mechanical micromanipulation of proteins and DNA possible and has provided a new way to probe the internal bonding mechanism in these biopolymers. Experimental results on several examples of protein and nucleic-acid systems [1–14] have recently been reported. Fundamentally, an intriguing question is whether intermediate stages observed in different protein denaturing processes would *always* have one-to-one correspondence to each other, in particular, to folding pathways in a ''normal,'' unforced environment. In an effort to demonstrate the relevance of forced unfolding to the folding pathway, Carrion-Vazques and co-workers [5] have compared mechanical and chemical denaturation of the I27 domain of the protein titin (a β-sheet rich native structure) and have concluded that they seem to have the same effects on the unfolding pathways. Desai and co-workers [12] have performed a pressure-jump experiment on the *trp* repressor (an α-helix rich native structure) and have observed no unfolding intermediates under high pressure.

Computer simulation studies of force-induced unfolding of proteins provide complementary information on the underlying microscopic physical picture of the denaturing process. Both all-atom and minimal models are useful for this purpose [15–27]. For example, Klimov and Thirumalai have used a lattice model [19] and later more realistic β-bundle models [20] to observe the unfolding intermediate stages when a protein is pulled by a force. The latter study indicates that thermal unfolding proceeds in all-or-none fashion, without any detectible intermediates. In contrast, force-induced unfolding of one of these models accompanies an observable intermediate. Paci and Karplus [21,22] have shown that the intermediate states detected in the forced unfolding simulations of all-atom protein models are not evidently related to the process observed in a thermal denaturing experiment as the temperature increases. While the studies of Paci and Karplus were carried out for systems containing no explicit water molecules, other groups have considered the presence of water molecules explicitly [15–18,26]. Lu *et al.* [15–17], for example, used steered molecular-dynamic simulations to predict the atomistic events during the forced extension of titn I27 domain. These simulations were successful in reproducing a force peak observed on the force-extension curve from atomic-force-microscope experiments. These simulations identified structural components responsible for a large bottleneck to unfolding of the I27 domain. A key event initiating domain unfolding consists of simultaneous and cooperative disassociation of hydrogen bonds, which connect the two β strands on the C and N termini to the other part of the protein. We have previously targeted at investigating the behavior of a β-sheet barrel model in the uniform and elongation flows [27], and found different unfolding scenarios. Best *et al.* [26] have studied unfolding of two proteins, barnase and I27 domain, and concluded that the force-induced intermediate states found in computer simulations are much more nativelike then those found by thermal denaturation simulations.

Hence, the important issue here is to what extent the intermediate states participate in these unfolding and folding events and whether they are related to refolding pathways. The above experiments and computer simulations seem to have pointed to different directions in answering these questions. It is our purpose in this paper to provide a clear physical picture and discuss the unfolding of two minimal protein models, an α-helix bundle [28] and a β-sheet barrel [29], under different types of denaturing environments: thermal heating, heat shock, in a uniform flow, and in an elongation flow, in order to give a more systematic comparison of the unfolding pathways experienced by the modeled proteins in a wider variety of unfolding environments. Our simulation results indicate that the unfolding pathways are critically dependent on the physical mechanics of how a protein is denatured. The relationship between forced unfolding pathways and the actual folding pathways is not always transparent.

We have chosen to study the minimal models by Thirumalai and co-workers [28,29] in our simulation. The simplicity of the model enables us to perform extensive sampling of the conformational space needed for an accurate calculation of the thermodynamic (heat capacity curves, phase diagrams, free-energy profiles) and kinetic (folding) properties of the system, which would otherwise be unfeasible in an all-atom approach. The richness of the resulting structures allows us to test various types of commonly occurring structures (α

*Author to whom correspondence should be addressed.

helix and β sheet) under different perturbing environments and to study the relationship between the force-induced and refolding intermediates. In particular, one additional advantage of using these two models is that their structural properties were previously well documented.

II. MODELS

There has been considerable progress, through the use of new and sophisticated simulation techniques, in recent years to predict protein structures without questioning the folding pathways [30]. To follow the kinetics of folding and unfolding of proteins, however, some of these new techniques are not applicable. Minimal models are more efficient in terms of computational time [19,20,24], although all-atom dynamic simulations are also available in literature [15–17,21].

The α-helix bundle and β-sheet barrel models of Thirumalai and co-workers are two extensively studied minimal models [28,29,31–34]. The native structures, corresponding to the minima of the potential energy, are illustrated on the top left of Figs. 1(a) and 1(b), respectively, for the α-helix bundle and β-sheet barrel. The α-helix bundle has 73 monomers and the β-sheet barrel has 46 monomers. Four segments of stable secondary structures are formed in each of these two models. The key components of the potential energy in both polymer models include terms that deal with the fluctuations of the bond angles about a fixed value, a heterogeneous long-range Lennard-Jones potential reflecting the three different types of residues, hydrophobic, hydrophilic, and neutral, and a torsional-angle potential that effectively prefers a local α-helix or β-sheet conformation [28,29]. Figure 1 demonstrates a series of representative structures as the temperature is lowered, together with the heat capacity and radius of gyration measurements that give signatures of the stability of the structures. The plots in Fig. 1 are based on our independent molecular-dynamics (MD) calculations by using the WHAM method [35]. In both models, there exists an intermediate state at a reduced temperature, $\tilde{T} \equiv T k_B / \epsilon \approx 0.6$, where the protein structure is partially bundled. In α-helix bundle, the intermediate state has a stable three helix bundle connected to a separated segment of well-formed helix. The minimum in the heat capacity between two peaks signifies the existence and stability of this intermediate. In β-sheet barrel, the intermediate state has a less stable three β-strand barrel connected to a separate segment. The segment displays coiled conformation and forms a β sheet if bonded to the β barrel. This intermediate state leaves no clear signature in the heat capacity plot and exists only as a kinetic folding intermediate as shown below. Here ϵ is a typical energy scale when two residues are bonded through a hydrophobic force.

A collision molecular-dynamics procedure [36] has been implemented to simulate the kinetics of folding and unfolding of these two model proteins. The temperature of the system is maintained effectively by collisions of the monomers in a protein model with virtual solvent particles carrying a kinetic energy that obeys the Boltzmann distribution. The collisional dynamics procedure allows for effective simulations of a hydrodynamic-flow environment. Throughout the simulations, a basic time step of $0.005 t_0$ was used, where $t_0 = \sigma (m/\epsilon)^{1/2}$ and σ and m are the excluded-volume diameter and mass of a monomer, respectively. The characteristics of the system such as energy E and radius of gyration R_g were collected during the simulation every 200 steps. A simple average of the collected system energy $\overline{E}$ is calculated for each specified R_g value, and produces the characteristic $\overline{E}$-R_g curve to be discussed below.

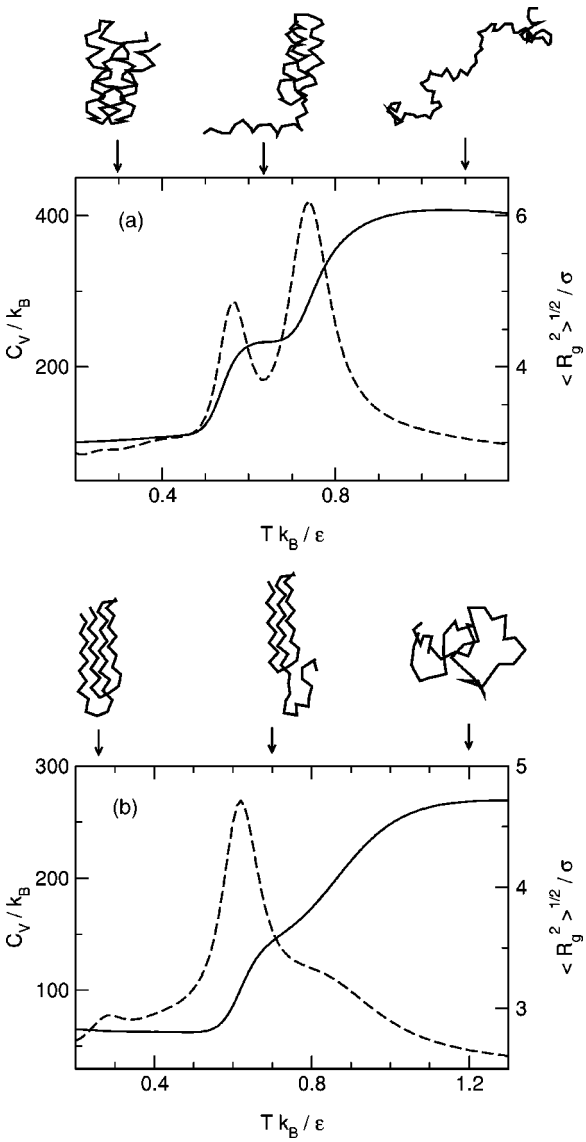

FIG. 1. Temperature dependence of the heat capacity C_v (dashed line to the left scale) and the average radius of gyration $\langle R_g^2 \rangle^{1/2}$ (solid line to the right scale) for the α-helix bundle (a) and β-sheet barrel (b) protein models. A schematic representation of the protein structures corresponding to different thermodynamic states is displayed on the top of each figure. The native states of the models, displayed at left of the plots, are a four-α-helix bundle and a four-β-strand barrel. The intermediate state in the middle of (a) is thermodynamically stable, as can be identified by the minimum in C_v. However, the intermediate state in the middle of (b) is thermodynamically less stable and leaves no traceable signatures in the C_v plot in (b). The latter is a kinetic intermediate (see text).

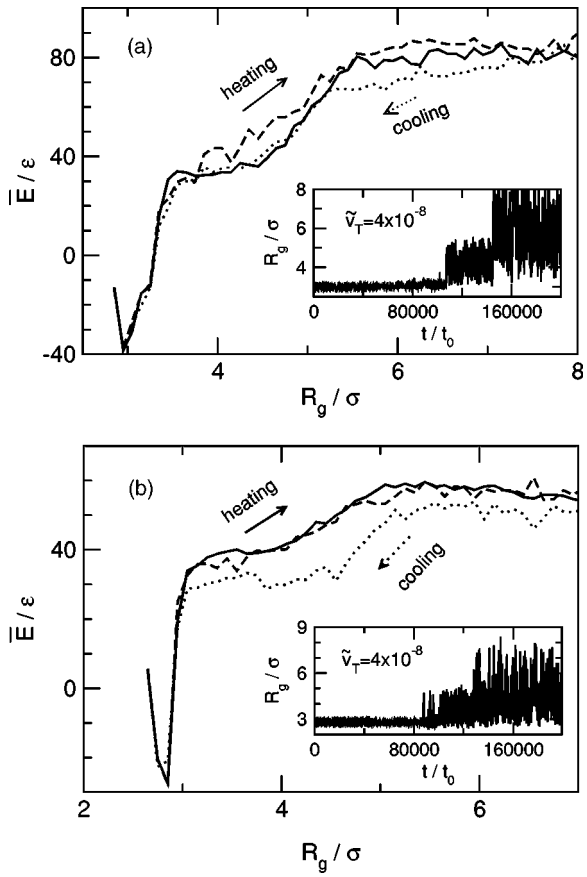

FIG. 2. Average energy $\bar{E}$ vs radius of gyration R_g calculated from three different MD trajectories of the α-bundle (a) and β-barrel (b) protein models. Solid and dashed lines correspond to the heating simulations in which the temperature of the system was increased continuously [see Eq. (1)] with a constant rate of $v_T=4\times10^{-8}$ and $v_T=9\times10^{-8}$ [plot (a)], $v_T=3\times10^{-8}$ and $v_T=11\times10^{-8}$ [plot (b)]. The dotted lines correspond to the cooling simulations in which the temperature was decreased continuously with a constant rate of $v_T=-4\times10^{-8}$. The insets show the time behavior of the radius of gyration in the heating simulations with $v_T=4\times10^{-8}$.

III. SIMULATION RESULTS

A. Thermal heating or cooling

In the first set of simulations, we slowly heat up the system by raising the temperature $\tilde{T}$ with a constant rate continuously from $\tilde{T}_0=0.1$ to 1.0 in the α-bundle model and from $\tilde{T}_0=0.1$ to 1.2 in the β-barrel model,

$$\tilde{T}(\tilde{t})=\tilde{T}_0+v_T\tilde{t}, \tag{1}$$

where $\tilde{t}$ is the time measured in terms of a MD step. At initial temperature $\tilde{T}_0$ the model proteins adopt the thermodynamically stable, native conformations. The final temperature is sufficiently high so that the model proteins can be clearly seen to adopt a random coil conformation (see the top right sketch in Fig. 1). The solid and long dashed curves in Figs. 2(a) and 2(b) demonstrate the heating $\bar{E}$-R_g characteristics of the two systems. For the α-bundle model, a heating rate of $v_T=4\times10^{-8}$ and 9×10^{-8} was used and for the β-barrel model, $v_T=3\times10^{-8}$ and 11×10^{-8}. These different heating rates, however, can been seen to produce no major differences in these plots. In both models, the $\bar{E}$-R_g characteristic curves are relatively smooth, with a hint of the stability of the intermediate state region near $R_g=4\sigma$ (see insets) when the temperature passes through $\tilde{T}=0.6$, a temperature corresponding to the stable region of such an intermediate structure. Due to the fact that the intermediate state is less thermodynamically stable in the β-barrel model, a less clear step is shown in the inset of Fig. 2(b).

In order to observe the annealed refolding, we slowly cool down the system by linearly decreasing the temperature $\tilde{T}$ continuously from $\tilde{T}_0=1.0$ to $\tilde{T}=0.2$ in both models with a cooling rate of $v_T=-4\times10^{-8}$ in Eq. (1). An initial random coil structure was used. The $\bar{E}$-R_g characteristics are demonstrated in Fig. 2 by dotted curves. In the β-barrel model, a plateau in the region near $R_g=4\sigma$ is clearly visible, which gives a signature of the kinetic stability of the intermediate state; energetically, the systems are trapped in these regions before an even lower energy can be attained. Such a trap, however, does not exist in the heating procedure where the protein can continuously unfold, giving rise to rather smooth characteristic curves.

B. Heat shock

In the second set of simulations, we consider systems in an initially native conformation at $\tilde{T}_0=0.1$ and instantaneously raise the temperature to $\tilde{T}_f$. This simulates a heat-shock experiment, in which an initial amount of heat is ejected into the solvent. The $\bar{E}$-$\tilde{T}$ characteristics for a few different values of $\tilde{T}_f$ are displayed in Fig. 3 and show featureless curves. The systems receive enough thermal energy to almost instantaneously denature into a structure that is characteristic to the stable state corresponding to the final temperatures. The time dependence of R_g, however, reveals *different* characteristics of the approach to the final equilibrium states. The inset in Fig. 3(a) shows R_g of the α-bundle model as a function of the simulation time, recorded with a final temperature $\tilde{T}=0.6$ at which the intermediate state shown in Fig. 1(a) is thermodynamically stable. Three of four helices are tightly packed forming a three-helix bundle. The fluctuations in the R_g-$\tilde{t}$ curve reflect the motion of the isolated, fourth helical segment that is more flexible in comparison to the native structure. The isolated segment displays a melted configuration, a nativelike helix, or a bent helical structure.

A different type of trajectory can be seen in the inset of Fig. 3(b) for the β-barrel model, recorded with the same final temperature. The fluctuations in the R_g-$\tilde{t}$ curve reflect the opening and closing motion of a β-strand segment that attempts to dissociate from the bundle structure formed by the other three β-strands. When it is in the unbound configuration the segment is in a coiled state and experiences a strong attraction to the remainder of the molecule. This attraction

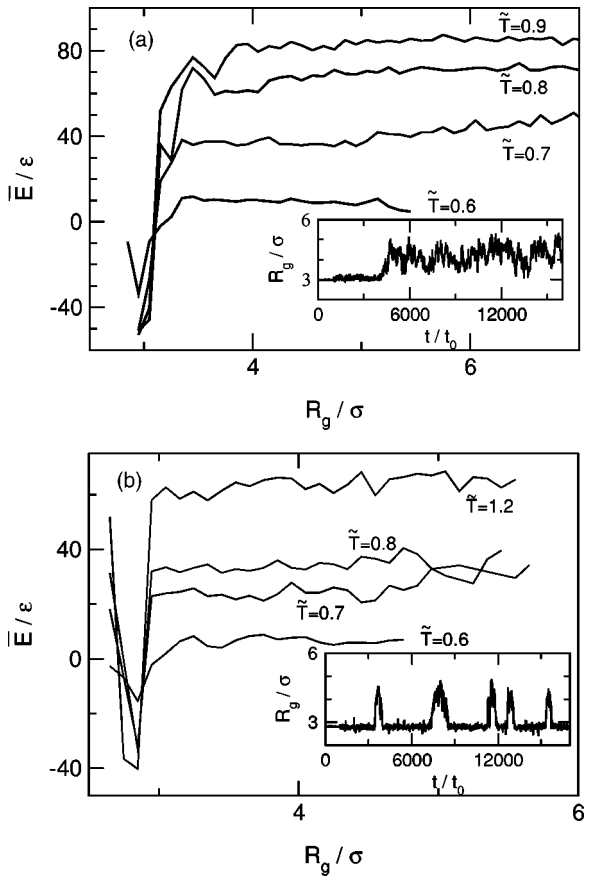

FIG. 3. Average energy $\bar{E}$ vs radius of gyration R_g obtained from the heat-shock MD simulations for the α-bundle (a) and β-barrel (b) protein models. Each curve describes a simulation in which the temperature of the system was suddenly increased from $\tilde{T}_0=0.1$ to various $\tilde{T}_f$ indicated on the graph. The insets show the radius of gyration as a function of time in the simulations in which an initial jump to the temperature $\tilde{T}_f=0.6$ occurs at $t=1000t_0$.

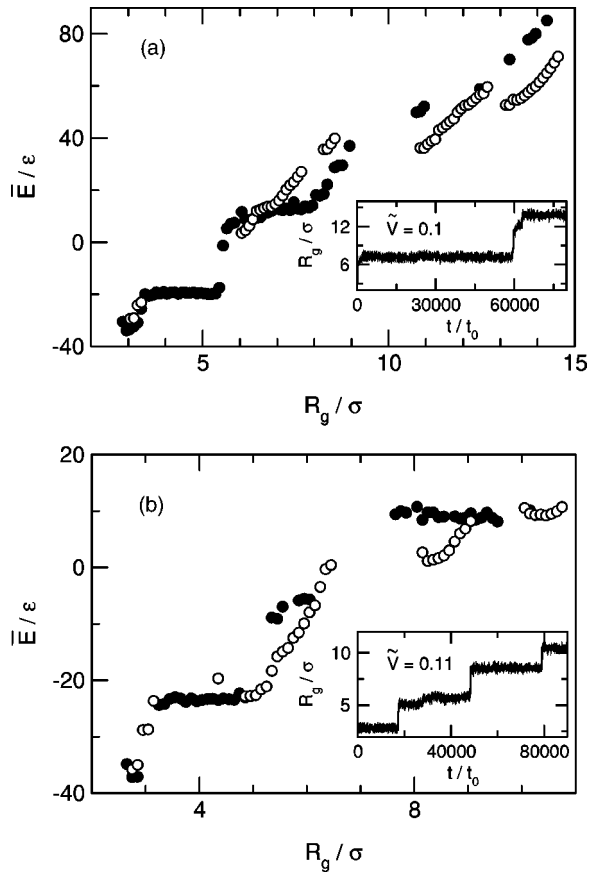

FIG. 4. Average energy $\bar{E}$ vs radius of gyration R_g for the α-bundle (a) and β-barrel (b) protein models in the uniform flow with velocities: (a) $\tilde{V}=0.1$ (open circles) and 0.0007 (filled circles); (b) $\tilde{V}=0.11$ (open circles) and 0.001 (filled circles). A native initial configuration is adopted in unfolding simulations (open circles) and a stretched initial configuration is adopted in refolding simulations (filled circles). The insets show the radius of gyration as a function of time in unfolding simulations at high flow velocities. In all these simulations, a terminal end of the protein is fixed in space.

leads to relatively fast rebounding of the segment. In the β-barrel model 59% of monomers are hydrophobic, whereas in the α-bundle model 33% of monomers are hydrophobic. Hence, the attraction between the hydrophobic core and the dissociated segment in the β-barrel model is stronger than that in the α-bundle model. That segment may fluctuate between two clearly defined states: a coil conformation (larger R_g) and a bonded conformation (smaller R_g).

C. Uniform flow

In the next set of simulations, the initial native structures of the modeled proteins were stretched in a simulated uniform flow environment at $\tilde{T}=0.1$ when the position of one of the terminal ends is fixed in space. We have chosen a velocity field of $\tilde{V}\equiv V_x t_0 \sigma^{-1}=0.1$ that is coupled to the velocity distribution of the virtual solvent particles [36]. We have shown elsewhere that this flow velocity adequately covers the entire stretching regime where the protein unfolds through more than one intermediate step [27]. The open circles in Fig. 4 represent the unfolding $\bar{E}$-R_g characteristics where a few plateaus can be seen in both plots. In comparison with the thermal denaturing simulations , the $\bar{E}$-R_g characteristics of both models show more features that are typical of a forced stretching experiment. In the vicinity of $R_g=4\sigma$, the system is denatured through an intermediate state described above. Since the system temperature is relatively low, the secondary structures remain almost intact until the final stretching stage. The steps occurring at large R_g are not seen in thermal denaturing simulations. The additional intermediate state contains a stretched segment corresponding to two original α-helix (or β-sheet) segments and a segment that still has a partial native conformation. The plateaus on $\bar{E}$-R_g curves reflect the stepwise unzipping of secondary structures from a native structure before a fully stretched conformation can be achieved. The plots in the insets of Fig. 4 show R_g as a function of simulation time, where the steps that R_g goes through are clearly visible.

Also plotted as filled circles in Fig. 4 are the $\bar{E}$-R_g characteristics of a refolding simulation where we have taken the

fully stretched structure from the above simulations and observed the refolding of the modeled protein back to its native structure in a flow with low velocity. Starting from the initial extended, straight-line-like configurations, proteins refold by going through various stages in an almost reverse order from the unfolding process.

D. Elongational flow

In the final set of simulations, we consider the unfolding of the modeled proteins in an extension flow. The flow pattern is arranged in such a way that the center of mass of the protein would experience no force on average and the flow velocity follows a spatial dependence:

$$w_x = \dot{\epsilon}(x - x_c), \quad w_y = -0.5\dot{\epsilon}(y - y_c), \quad w_z = -0.5\dot{\epsilon}(z - z_c), \tag{2}$$

where (x_c, y_c, z_c) is the location of the center of mass and $\dot{\epsilon}$ is the elongation rate. To our surprise, proteins in the extensional flow behave very differently in comparison to the previous stretching scheme. There exists a critical flow rate, $\dot{\epsilon}_c \approx 0.1 t_0^{-1}$, below which we see a small nonsignificant distortion of the native conformation. Above the critical elongation rate, the model protein would attain an almost fully stretched conformation abruptly, going through no intermediate steps. The open triangles at the low left corners of Fig. 5(a) and Fig. 5(b) represent the initial conformation of the proteins. With an overcritical flow rate, large R_g values can be obtained almost instantaneously as soon as the transition occurs. The inset in Fig. 5 further describes this behavior as the radius of gyration jumps to a fully stretched value. In comparison to this all-or-none scenario, the insets in Fig. 4 describe how intermediate steps are observed in a uniform flow. We have also performed refolding simulations in these systems by letting the final extended configuration to refold back to the native structure at a low elongation-rate. The filled triangles in Fig. 5 demonstrate the $\overline{E}$-R_g characteristics of the refolding process. There is virtually no difference in comparison to the refolding curves obtained from the uniform-flow simulations. The refolding simulations were started from a similar, fully stretched state.

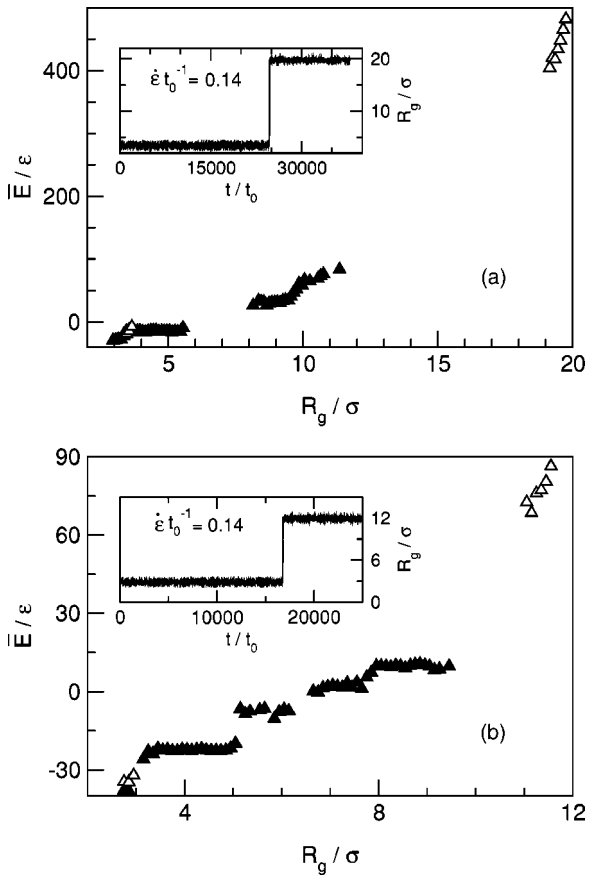

FIG. 5. Average energy $\overline{E}$ vs radius of gyration R_g for the α-bundle (a) and β-barrel (b) protein models in an elongational flow with different elongational rates: (a) $\dot{\epsilon}=0.14$ (open triangles) and 0.0003 (filled triangles); (b) $\dot{\epsilon}=0.14$ (open triangles) and 0.001 (filled triangles). A native initial configuration is adopted in unfolding (open triangles) and a stretched initial configuration is adopted in refolding (filled triangles). The insets show the radius of gyration as a function of time in unfolding simulations at a high elongational rate.

IV. DISCUSSIONS

To summarize, we have carried out computer simulations to observe the denaturing of two protein models under various environments. Although force-extension curves are more common in an experiment involving a manipulating force, we used the energy-extension characteristic curves to demonstrate the different unfolding mechanisms because of the fact that potential energy is a well-defined physical quantity in all four types of simulations carried out here.

Our first conclusion is that proteins yield different unfolding intermediate stages that are not necessarily the same as the thermodynamically stable intermediate state. One notable result is that these intermediate states are completely absent in the elongational-flow simulation and heat-shock simulation. The dominating physical mechanisms are similar in these two cases: every monomer receives an average kinetic energy that is high enough to delocalize it from the a bonding site.

The thermodynamic intermediate states are clearly visible in both low-rate heating and cooling simulations where every monomer receives a small amount of kinetic energy and the systems slowly evolve into the final stage. At each time step, the systems are in quasiequilibrium. One of the features in the cooling experiment is that the intermediate state is reached at a relatively low temperature and hydrophobic contacts in the intermediate state can energetically trap the protein. Hence, a more clear intermediate step in the characteristic curve is formed.

The computer simulations of the I27 domain using implicit and explicit solvent models [15–17,22] have indicated an unfolding ''bottleneck,'' i.e., an intermediate state. MD simulations of these all-atom models of the I27 domain also revealed an energy landscape with extra minima. A comparable situation exists here (see Fig. 2).

A different perspective of the folding and refolding simulations in a uniform flow can be gained with a reference frame moving with the flow. The fixed end becomes a moving monomer pulled by a force. No other monomers experience direct pulling force. The segments that are immediately connected to the moving monomer experience an indirect force due to the pulling. Hence, the pulling force rips the protein apart segment by segment, with possible native domains still kept intact. A protein in a uniform flow or a protein pulled by one end thus exhibits richer unzipping intermediate states than that of a thermal denaturing experiment.

Though not conclusive, as we only studied two protein models, we suggest that the differences in the characteristic plots are caused by the different denaturing processes, not by the difference in the internal structure of proteins. The intermediate states of the two models actually have different thermodynamic properties: stable in α-helix bundle and less stable in β-sheet barrel. These intermediate states, however, play a crucial role kinetically in the formation of the native structures [29,31]. Uniform flow and thermal denaturing simulations reveal the intermediate states more clearly.

In principle, flow induced unfolding of proteins can be directly performed experimentally and this will provide a basis for comparison to some of our conclusions here. To our knowledge, however, only DNA molecules have been considered previously in such experiments. In different hydrodynamic flows, Chu and co-workers have provided a mechanism of direct visualization of DNA conformations [13,37,38] using laser tweezers.

Financial support for this work was provided by the Natural Science and Engineering Research Council of Canada.

[1] T. E. Fisher, P. E. Marszalek, and J. M. Fernandez, Nat. Struct. Biol. **7**, 719 (2000).
[2] M. Rief, M. Gautel, F. Oesterhelt, J. M. Fernandez, and H. E. Gaub, Science **276**, 1109 (1997).
[3] M.S.Z. Kellermayer, S.B. Smith, H.L. Granzier, and C. Bustamante, Science **276**, 1112 (1997).
[4] L. Tskhovrebova, J. Trinick, J. A. Sleep, and R. M. Simmons, Nature (London) **387**, 308 (1997).
[5] M. Carrion-Vazquez, A. F. Oberhauser, S. B. Fowler, P. E. Marszalek, S. E. Broedel, J. Clarke, and J. M. Fernandez, Proc. Natl. Acad. Sci. U.S.A. **96**, 3694 (1999).
[6] P. E. Marszalek, H. Lu, H. B. Li, M. Carrion-Vasquez, A. F. Oberhauser, K. Schulten, and J. M. Fernandez, Nature (London) **402**, 100 (1999).
[7] A. F. Oberhauser, P. E. Marszalek, H. P. Erickson, and J. M. Fernandez, Nature (London) **393**, 181 (1998).
[8] M. Carrion-Vasquez, P. E. Marszalek, A. F. Oberhauser, and J. M. Fernandez, Proc. Natl. Acad. Sci. U.S.A. **96**, 11 288 (1999).
[9] H. B. Li, A. F. Oberhauser, S. B. Fowler, J. Clarke, and J. M. Fernandez, Proc. Natl. Acad. Sci. U.S.A. **97**, 6527 (2000).
[10] A. D. Mehta, M. Rief, J. A. Spudich, D. A. Smith, and R. M. Simmons, Science **283**, 1689 (1999).
[11] H. P. Erickson, Science **276**, 1090 (1997).
[12] G. Desai, G. Panick, M. Zein, R. Winter, and C. A. Royer, J. Mol. Biol. **288**, 461 (1999).
[13] T. T. Perkins, D. E. Smith, R. G. Larson, and S. Chu, Science **268**, 83 (1995).
[14] S. B. Smith, L. Finzi, and C. Bustamante, Science **258**, 1122 (1992).
[15] H. Lu, B. Isralewitz, A. Krammer, V. Vogel, and K. Schulten, Biophys. J. **75**, 662 (1998).
[16] H. Lu and K. Schulten, Chem. Phys. **247**, 141 (1999).
[17] H. Lu and K. Schulten, Biophys. J. **79**, 51 (2000).
[18] A. Krammer, H. Lu, B. Isralewitz, K. Schulten, and V. Vogel, Proc. Natl. Acad. Sci. U.S.A. **96**, 1351 (1999).
[19] D. K. Klimov and D. Thirumalai, Proc. Natl. Acad. Sci. U.S.A. **96**, 6166 (1999).
[20] D. K. Klimov and D. Thirumalai, Proc. Natl. Acad. Sci. U.S.A. **97**, 7254 (2000).
[21] E. Paci and M. Karplus, Proc. Natl. Acad. Sci. U.S.A. **97**, 6521 (2000).
[22] E. Paci and M. Karplus, J. Mol. Biol. **288**, 441 (1999).
[23] Z. Bryant, V. S. Pande, and D. S. Rokhsar, Biophys. J. **78**, 584 (2000).
[24] D. N. Socci, J. N. Onuchic, and P. G. Wolynes, Proc. Natl. Acad. Sci. U.S.A. **96**, 2031 (1999).
[25] D. Craig, A. Krammer, K. Schulten, and V. Vogel, Proc. Natl. Acad. Sci. U.S.A. **98**, 5590 (2001).
[26] R. B. Best, B. Li, A. Steward, V. Daggett, and J. Clarke, Biophys. J. **81**, 2344 (2001).
[27] A. S. Lemak, J. R. Lepock, and J. Z. Y. Chen, Proteins (to be published).
[28] J. D. Honeycutt and D. Thirumalai, Biopolymers **32**, 695 (1992).
[29] Z. Guo and D. Thirumalai, J. Mol. Biol. **263**, 323 (1996).
[30] U. H. E. Hansmann and Y. Okamoto, Physica A **99**, 415 (1994).
[31] Z. Guo and D. Thirumalai, Biopolymers **36**, 83 (1995).
[32] Z. Guo and C. L. Brooks III, Biopolymers **42**, 745 (1997).
[33] J.-E. Shea, Y. D. Nochomovitz, Z. Guo, and C. L. Brooks III, J. Chem. Phys. **109**, 2895 (1998).
[34] H. Nymeyer, A. E. Garcia, and J. N. Onuchic, Proc. Natl. Acad. Sci. U.S.A. **95**, 5921 (1998).
[35] S. Kumar, D. Bouzida, R. H. Swendsen, P. A. Kollman, and J. M. Rosenberg, J. Comput. Chem. **13**, 1011 (1992).
[36] A. S. Lemak and N. K. Balabaev, J. Comput. Chem. **17**, 1685 (1996).
[37] T. T. Perkins, D. E. Smith, and S. Chu, Science **276**, 2016 (1997).
[38] D. E. Smith and S. Chu, Science **281**, 1335 (1998).